JES Focus Issue of Selected Papers from IMLB 2018

The Effect of Electrode-Electrolyte Interface on the Electrochemical Impedance Spectra for Positive Electrode in Li-Ion Battery

Ryoichi Tatara,[1,*,z] Pinar Karayaylali,[2] Yang Yu,[3] Yirui Zhang,[2] Livia Giordano,[1,2,4] Filippo Maglia,[5] Roland Jung,[5] Jan Philipp Schmidt,[5] Isaac Lund,[6] and Yang Shao-Horn[1,2,3,,z]**

[1]*Research Laboratory of Electronics, Massachusetts Institute of Technology, Cambridge, Massachusetts 02139, USA*
[2]*Department of Mechanical Engineering, Massachusetts Institute of Technology, Cambridge, Massachusetts 02139, USA*
[3]*Department of Material Science and Engineering, Massachusetts Institute of Technology, Cambridge, Massachusetts 02139, USA*
[4]*Department of Material Science, Università di Milano-Bicocca, 20136 Milan, Italy*
[5]*BMW Group, 80788 München, Germany*
[6]*BMW Group Technology Office USA, Mountain View, California 94043, USA*

Understanding the effect of electrode-electrolyte interface (EEI) on the kinetics of electrode reaction is critical to design high-energy Li-ion batteries. While electrochemical impedance spectroscopy (EIS) is used widely to examine the kinetics of electrode reaction in Li-ion batteries, ambiguities exist in the physical origin of EIS responses for composite electrodes. In this study, we performed EIS measurement by using a three-electrode cell with a mesh-reference electrode, to avoid the effect of counter electrode impedance and artefactual responses due to asymmetric cell configuration, and composite or oxide-only working electrodes. Here we discuss the detailed assignment of impedance spectra for $LiCoO_2$ as a function of voltage. The high-frequency semicircle was assigned to the impedance associated with ion adsorption and desorption at the electrified interface while the low-frequency semicircle was related to the charge transfer impedance associated with desolvation/solvation of lithium ions, and lithium ion intercalation/de-intercalation into/from Li_xCoO_2. Exposure to higher charging voltages and greater hold time at high voltages led to no significant change for the high-frequency component but greater resistance and greater activation energy for the low-frequency circle. The greater charge transfer impedance was attributed to the growth of EEI layers on the charged Li_xCoO_2 surface associated with electrolyte oxidation promoted by ethylene carbonate dehydrogenation.

Manuscript submitted October 1, 2018; revised manuscript received November 7, 2018. Published November 27, 2018. *This paper is part of the JES Focus Issue of Selected Papers from IMLB 2018.*

Improving kinetics of electrochemical reaction is the key to design high-performance battery systems for electrical vehicles and other applications. Electrochemical reactions proceed at the interface of electrode and electrolyte, yet there is still limited understanding on how different components of electrode-electrolyte interface (EEI) affects the kinetics of the charge transfer reactions.[1] For instance, carbonate-based electrolytes, which are most commonly used for Li-ion batteries, are well known to be reduced at the negative electrode surface to form the solid-electrolyte-interphase (SEI).[2] On the other hand, these carbonate-based electrolytes can also be oxidized at the oxide surface in the positive electrode to form EEI layer even at ~4.1 V_{Li}, within operating potentials of Li-ion batteries.[3,4] In addition, introducing late transition metals such as Ni in the layered oxides materials (e.g. $LiNi_xMn_yCo_{1-x-y}O_2$) enhances electrolyte oxidation as reported recently.[5–7] Such electrolyte oxidation generates reaction products formed on the electrode surface, which can increase cell resistance and decrease cycle life.[1] However, the formation mechanism and chemical composition of EEI layer that governs the lithium ion transport and/or kinetics of lithium intercalation/de-intercalation at the electrode surface are not well-understood.

Recent density functional theory (DFT) work shows that the thermodynamic driving force for the dissociative adsorption of ethylene carbonate (EC) on the oxide surface such as Li_xMO_2 increases with lowering the Fermi level into the O 2*p* band,[4] induced by lithium de-intercalation and the use of late transition metal in Li_xMO_2. The dissociative adsorption of EC (dehydrogenation of EC) produces acidic OH group on the oxide surface, which can further react with electrolyte salt such as $LiPF_6$. Recent XPS studies[3] on carbon-free, binder-free Li_xCoO_2 show a marked growth of oxygenated and carbonated species along with the increase of LiF and $Li_xPF_yO_z$ species upon charging of $LiCoO_2$. In addition, the correlation between the interface composition and the thermodynamic driving force of dissociative adsorption of EC on $LiCoO_2$ surface has been also discussed via DFT calculation: preferential reaction of surface OH group, being energetically more favorable with increasing state-of-charge, with $LiPF_6$ to form LiF and $Li_xPF_yO_z$ species probed through XPS, as well as HF and $PF_2O_2^-$ solution species probed by NMR. However, the impact of EEI grown on the Li_xCoO_2 surface on the kinetics of intercalation and de-intercalation and electrode impedance is not well understood.

While electrochemical impedance spectroscopy (EIS) has been used to study the kinetics of positive electrode in Li-ion batteries since 1985,[8] ambiguities still exist in the physical origin and the assignments of EIS features, especially for composite electrodes. Generally speaking, two of the semicircles appeared in the Nyquist plots for lithium intercalation/deintercalation reaction into composite electrodes such as $LiCoO_2$ in 1 mol/L $LiBF_4$ in propylene carbonate,[8] $LiMn_2O_4/LiNiO_2/LiCoO_2$ in 1 mol/L $LiAsF_6$ in ethylene carbonate (EC) -dimethyl carbonate (DMC) (1:3),[9] $LiNi_{1/3}Mn_{1/3}Co_{1/3}O_2$ in 1 mol/L $LiPF_6$ in ethylene carbonate: diethyl carbonate (DEC) (1:1 vol),[10] graphite in 1 mol/L $LiAsF_6$ in EC-DMC (1:3),[11] and graphite in ionic liquids,[12] etc.[13–21] Previous studies have proposed that the high-frequency components correspond to surface or EEI layer resistance.[8,9,11,15,18] For example, Goodenough et al.,[8] and Aurbach et al.,[9] reported high-frequency semicircles in composite

*Electrochemical Society Member.
**Electrochemical Society Fellow.
[z]E-mail: shaohorn@mit.edu; tatara@mit.edu

positive electrodes was assigned for surface film formation according to modeling results and insensitivity against electrode potential. In contrast, Choi et al.,[13] have reported that high-frequency semicircle can be assigned to particle/particle contact resistance in the composite electrodes of $LiNiO_2/LiCoO_2$ in 1 mol/L $LiClO_4$ in PC while Lindbergh et al.,[14] have reported that it corresponds to the contact resistance between electrode and current collector (reported with $LiMn_2O_4$ in $LiClO_4/LiBF_4$ in carbonate solutions). The discrepancies may arise from overlapped responses from negative and positive electrodes in two-electrode cells[22–24] used for EIS measurements or artefactual EIS response from three-electrode cells with asymmetric cell configurations due to equipotential line distortion during frequency sweep.[25–27] In addition, the low-frequency component has been attributed to charge transfer resistance associated with lithium intercalation/de-intercalation,[8,11,18] which has voltage-dependent impedance.[9,15] On the other hand, Uchimoto et al.,[28] and Dokko et al.,[29] have reported only one voltage-dependent semicircle appeared on thin film and single particle Li_xCoO_2 electrodes (without binder and carbon), which could originate from charge transfer impedance at the Li_xCoO_2/electrolyte. As EEI films can form on thin film or single particle Li_xCoO_2 electrodes with increasing voltage,[3] the formation of EEI films on Li_xCoO_2 might not generate a separate EIS semicircle from the semicircle from charge transfer impedance in contrast to previous studies,[8,9,11,15,18] which requires further clarification.

In this study, we fabricated three-electrode cells customized for EIS measurements with a symmetric configuration to avoid artefacts in the EIS response. High-frequency and low-frequency EIS features of $LiCoO_2$ composite electrodes were examined as a function of charging voltage and aging time. The high-frequency semicircle is assigned to the impedance at the electrified interface, involving ion adsorption/desorption on the particle surface coupled with electron transfer to the surface of Li_xCoO_2 in the composite electrode, which is supported by decreasing resistance with increasing compress pressure and electrolyte ionic conductivity. On the other hand, the low-frequency semicircle corresponds to the kinetics of charge transfer associated with de-solvating/solvating lithium ions and lithium intercalation/de-intercalation into/from Li_xCoO_2. Increasing charging voltages above 4.4 V_{Li} and aging time at 4.4 V_{Li} and higher leads to greater resistance for high-frequency and low-frequency components as well as its activation energy, which can be attributed to EEI layer growth.

Experimental

Electrode preparation.—The positive electrode was composed of $LiCoO_2$ (85 wt%, synthesized according to the previously published procedure)[3] as an active material, carbon black (5 wt% KS6 and 2 wt% Super P, both from Timcal) as an electrically conductive additive, and poly(vinylidene fluoride) (8 wt%, PVDF, Kynar) as a binder polymer. The mesh reference electrode was also composed of 80 wt% of $Li_4Ti_5O_{12}$ (Itasco, >99.5%), 10 wt% of acetylene black (C-55, Chevron) and 10 wt% of PVDF. These materials were mixed together and thoroughly agitated in *N*-methylpyrrolidone (NMP, Aldrich). The obtained slurry was applied with a blade applicator onto aluminum foil (for $LiCoO_2$, 16 μm thickness) or 316 stainless-steel mesh (for $Li_4Ti_5O_{12}$, 325 × 325 mesh, opening size 0.0017"), and resulting sheet/mesh were dried at 70°C. Next, each electrode was punched with a 1/2 inch diameter (1.27 cmϕ) for $LiCoO_2$ and 18 mm diameter for $Li_4Ti_5O_{12}$ mesh reference. Carbon-free, binder-free $LiCoO_2$ electrodes were prepared by mixing $LiCoO_2$ with NMP in a 1:100 mass ratio. After ultrasonication for 5 minutes, the ink was deposited on 1/2 inchϕ (1.27 cmϕ) aluminum discs and dried at 100°C. The $LiCoO_2$ composite and carbon-free, binder-free electrodes were compressed at 6.3 T/cm^2 (unless otherwise noted) using a hydraulic press to improve electrical conductivity. All of the electrodes were further dried in vacuum at 80°C prior to cell assembling. The active material loading was ∼2.4 mg/cm^2 (∼8 μm thickness) for $LiCoO_2$ and ∼1.0 mg/cm^2 for $Li_4Ti_5O_{12}$ respectively unless otherwise noted. After compression at 6.3 T/cm^2, packing density of $LiCoO_2$ composite electrode is ca. 3.0 $g_{LCO\text{-}C\text{-}PVDF}$/cm^3 and porosity is ∼28% (without compression: ca. 2.0 $g_{LCO\text{-}C\text{-}PVDF}$/cm^3 and ∼52%). Particle size of synthesized $LiCoO_2$ was examined with a scanning electron microscope (JEOL 5910, with secondary electron detector at accelerating voltage of 15 kV) and shown in Figure S1 ($d \sim 1$ μm).

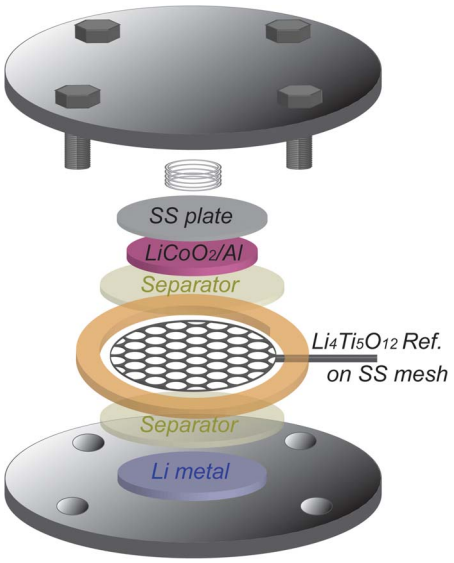

Figure 1. Schematic of three electrode EIS cell, where a mesh $Li_4Ti_5O_{12}$ reference electrode is placed between positive and negative electrode with two separators.

Electrochemical impedance spectroscopy (EIS).—Three-electrode cell was assembled in an argon-filled glove box ([H_2O], [O_2] < 0.5 ppm, MBraun) with a Li metal foil (15 mmϕ), 2 pieces of Celgard 2325 (19 mmϕ, MTI) as the separators, $Li_4Ti_5O_{12}$ mesh reference electrode (18 mmϕ), 2 pieces of Celgard 2325 (19 mmϕ) again, and $LiCoO_2$ electrode (1/2 inchϕ) from bottom to top, where a mesh $Li_4Ti_5O_{12}$ reference electrode was placed between positive and negative electrode with two separators (Figure 1). Mesh reference electrode was used to avoid inhomogeneous electric field during EIS measurement, which is known to cause artifactual EIS response (e.g. "spiral" behavior on Nyquist plots with Li rod reference electrode).[25,26,30,31] Mesh reference electrode also enables us to avoid blocking ion-flow/migration between positive and negative electrodes. In addition, loading density of $Li_4Ti_5O_{12}$ on mesh reference electrode is kept relatively low (∼1.0 mg/cm^2) to avoid impedance contribution from reference electrode.[25,26] It is known that the mesh reference impedance may be observed as additional processes in the measurement due to partially blocking ion-flow/migration in the electrolyte if loading density is too high impeding rigorous analysis.[25] 200 μL of 1 mol/L $LiPF_6$ in a 3:7 wt:wt ethylene carbonate (EC): ethyl methyl carbonate (EMC) electrolyte (LP57, BASF) was used as electrolyte. For preparing 0.1 mol/L and 0.01 mol/L $LiPF_6$ in EC-EMC (3:7 wt/wt) solutions, LP57 was simply diluted by pure EC (BASF) and EMC (BASF). Galvanostatic and potentiostatic charge and EIS tests were performed using VMP3 (potentiostat with frequency response analyzer, Biologic) with thermally equilibrated by thermostat chamber (SU-241, Espec) at 25°C. After cell assembly, $Li_4Ti_5O_{12}$ mesh reference electrode was electrochemically lithiated (negatively polarized at constant current of 500 μA against Li metal counter electrode with cutoff voltage of 1.3 V_{Li}) and got stable reference electrode potential at 1.56 V_{Li}.[26] Then $LiCoO_2$ working electrode was charged with different end-of-charge potential (3.9–4.6 V_{Li}) at 27.2 mA/g (0.1C rate based on theoretical capacity of 272 mAh/g, which corresponds to full lithium deintercalation: $LiCoO_2 \rightarrow Li^+ + e^- + CoO_2$.

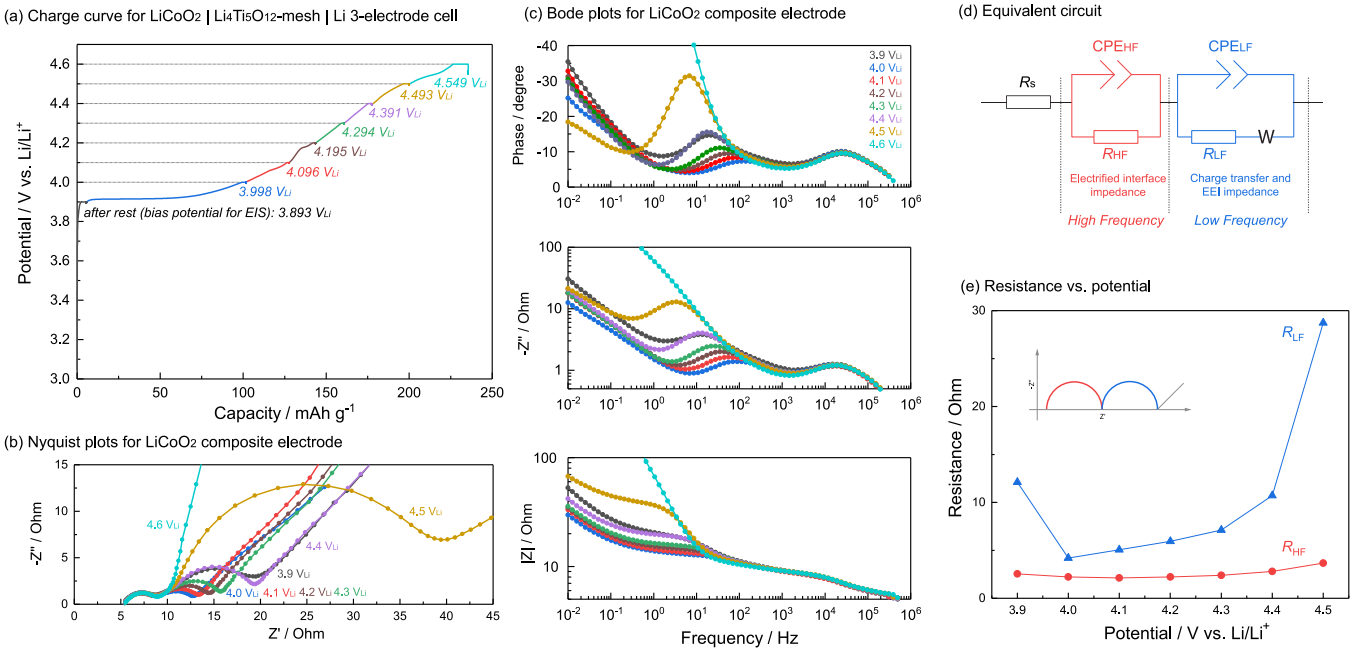

Figure 2. EIS measurement on $LiCoO_2$ composite electrode in $LiCoO_2$|$Li_4Ti_5O_{12}$-mesh|Li three electrode cell with 1 mol/L $LiPF_6$/EC-EMC (3:7 wt/wt) as electrolyte at different potential at 25°C; (a) charge curve, (b) Nyquist plots, (c) Bode plots, (d) equivalent circuit used to model obtained impedance spectra and (e) resistance vs. potential plots (detail fitting results are available in Figure S2). Cell was galvanostatically charged at 27.2 mA/g (0.1C) and hold potential for 1 hour at each potential, then relax 1 hour before EIS sequence. The $LiCoO_2$ loading is 2.4 mg/cm^2 and $LiCoO_2$ electrode was compressed at 6.3 T/cm^2.

27.2 mA/g corresponds to ~65 μA/cm^2 for average loading density of ~2.4 mg/cm^2), hold end-of-charge potential for 1 hour, and relax for 1 hour. After relax, EIS measurements were carried out at open circuit potential with 10 mV amplitude and frequency range from $\sim 10^{-2}$ to 10^6 Hz. For temperature dependence experiment, first the cell was charged with each end-of-charge potential at 25°C, then the cell was kept at each temperature (10–50°C) for 1 hour before EIS measurement. Obtained EIS data (excluded very high frequency region > 100 kHz if needed) were analyzed using ZView2 (Scribner). Ionic conductivity of electrolyte solution was measured using Traceable 23226-505 conductivity meter with thermostat chamber (SU-241, Espec).

X-ray photoelectron spectroscopy (XPS).—Cells after charging tests were disassembled in the glove box and the electrodes were gently rinsed with 100 μL of EMC and dried at room temperature under vacuum in the glove box antechamber for 3 h. Pristine and charged samples were transferred from the glove box to the XPS chamber of the spectrometer using a sample transfer vessel (ULVAC-PHI, INC.) avoiding exposure of the sample to air. All the XPS spectra were collected using a PHI 5000 Versa Probe II (ULVAC-PHI, INC.) using a monochromatized Al Kα source and a charge neutralizer. All spectra were recorded with a pass energy of 23.5 eV and calibrated with the C1s photoemission peak of adventitious carbon at 285 eV. After subtraction of a Shirley-type background, photoemission lines were fitted using combined Gaussian-Lorentzian functions. To facilitate comparison between samples, all the spectra were normalized by fixing the C1s photoemission peak of adventitious carbon (285 eV) to the same value. It is worth noted that, XPS collected from composite electrode generally have limited information due to the presence of conductive carbon and PVDF.[1,3,32] Conductive carbon, which has higher surface area than active material, might interact/react with electrolyte during charging reaction.[32] Furthermore, both conducting carbon and PVDF have strong band appeared in core spectra such as C1s, O1s and F1s, causing severe overlap with those from EEI layer. To avoid those ambiguities, XPS for carbon-free, binder-free electrodes or thin film electrodes would be the strong solutions,[3] however, to simply study the effect of EEI layer growth to EIS response here, we conducted XPS analysis for $LiCoO_2$ composite electrodes.

Results and Discussion

Assignment of EIS features of Li_xCoO_2 composite electrodes.—Figure 2a shows charge curves obtained for the $LiCoO_2$ composite electrode in 1 mol/L $LiPF_6$ in a 3:7 (wt:wt) EC: EMC solution with mesh $Li_4Ti_5O_{12}$ reference electrode and Li metal counter electrode. The main lithium deintercalation plateau ($LiCoO_2 \rightarrow xLi^+ + xe^- + Li_{1-x}CoO_2$) appeared from 3.9 V_{Li}, and potential gradually increases up to 4.6 V_{Li}, with showing charge capacity of 236 mAh/g. Both of plateau potential and charge capacity are consistent with previously reported results.[3,33,34] The depression of plateau around 4.15 V_{Li} can result from a phase transition between ordered and disordered Li^+ ion arrangements in the Li_xCoO_2 framework.[29] After potential holding at 3.9–4.5 V_{Li} for 1 hour and open circuit relaxation for one hour, observed voltage drop upon relaxation was within 10 mV, indicating that charged electrodes after potential holding is close to equilibrium. At 4.6 V_{Li}, voltage drop was larger than other voltages, implying larger voltage relaxation due to higher overpotential (slower kinetics) or the onset of self-discharge associated with electrolyte decomposition.[35] Figures 2b and 2c shows Nyquist and Bode plots for different potentials, where high-frequency (left on Nyquist plots) semicircle, low-frequency (right) semicircle and Warburg impedance at very low-frequency were observed consistent with previous work.[8,9,21] The size of low-frequency semicircle decreases with potential increasing from 3.9 to 4.0 V_{Li}, and increases again from 4.0 V_{Li} to 4.5 V_{Li}, while the size of high-frequency semicircle keeps almost constant among entire potential range.

Measured EIS spectra were analyzed quantitatively using an equivalent circuit shown in Figure 2d, which was made as physically simple as possible by considering numerous equivalent circuits reported previously.[8–11,30,36–38] In the equivalent circuit, R_s is the resistance of the bulk electrolyte solutions, $R_{HF, LF}$ and $CPE_{HF, LF}$ are resistance and

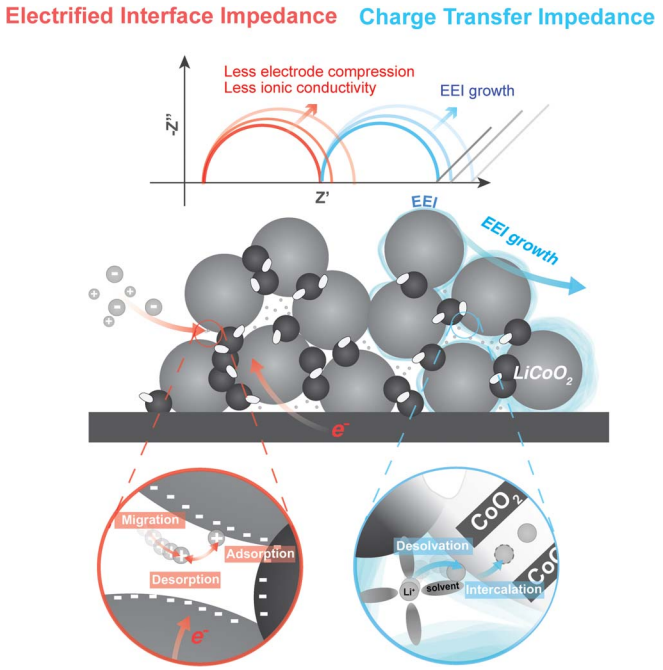

Figure 3. Schematic illustration for proposed assignment of EIS spectra. High-frequency (left) semicircle can be assigned to electrified interface impedance in the composite structure, which is combination of electron conduction in the composite electrode and Li^+ ion adsorption/desorption on the surface of composite electrode pore structure. Low-frequency (right) semicircle corresponds to combination of charge transfer resistance of Li_xCoO_2 and surface EEI layer resistance. As EEI layer grows, low-frequency (right) semicircle gets larger due to increase of EEI resistance, as well as increase of its activation energy.

constant phase element at high- and low-frequency range, and W is finite space (open) Warburg impedance, which reflects diffusion of Li^+ in the solid.[10] The fitted parameters of interest are summarized in Figure 2e and detailed fitting results are available in Figure S2. High-frequency (left) semicircle (R_{HF}) was found not to change so much through entire potential range, consistent with previous reports.[9] On the other hand, R_{LF} was found to first decrease from 3.9 to 4.0 V_{Li}, showing minimum at 4.0 V_{Li}, and then increases with increasing voltage up to 4.5 V_{Li}. The changes in the low-frequency semicircle resistance can be assigned to charge transfer kinetics.[9,39–42] Decreasing trend from 3.9 to 4.0 V_{Li} can be correlated with electrical conductivity enhancing through lithium deintercalation of $LiCoO_2$,[29,41] while increasing trend through further potential increase from 4.0 to 4.5 V_{Li}, especially sudden increase at 4.5 V_{Li}, might be simply come from end-of-charge, or surface film formation (at EEI layer) at high voltage (further discuss later). This assignment is further supported by previous work of thin-film electrode or single particle electrode, which exhibits one potential-dependent semicircle with comparable frequencies with those of low-frequency semicircles ($10^0 \sim 10^2$ Hz as shown in peak top frequency of imaginary impedance -Z'' in Figure 2c),[28,29,43,44] The size of semicircle observed in thin film and single particle electrode increases with potential holding or cycling even measured at the same potential as Li_xCoO_2 electrodes of this study.[29,43] Therefore, it is reasonable to assign low-frequency semicircle observed in Li_xCoO_2 composite electrodes, to combination of charge transfer and EEI layer resistance. As for high-frequency semicircle in composite electrode, here we assign it to the impedance of electrified interface between the composite electrode structure and the electrolyte, involving lithium ion adsorption/desorption on the surface of composite electrode coupled with electron transfer and migration in the composite electrode, as shown in Figure 3.

Further support to the EIS assignments came from EIS measurements with different compression pressures and electrolyte ionic conductivity. Figure 4a shows Nyquist plot obtained at 4.0 V_{Li} with the electrodes (with a fixed loading ~2.4 mg/cm^2) compressed at 6.3 T/cm^2, 0.79 T/cm^2 and without pressing. The size of high-frequency (left) semicircle was shown to decrease with increasing compression pressure, which is in good agreement with reduced composite electrode electronic resistance as expected at high compressing pressures. It is also reported that reducing active material particle size increases R_{HF},[10] which increases the number of particle/particle, particle/current collector and particle/electrolyte boundary. On the other hand, Figure 3b shows Nyquist plots with different $LiPF_6$ concentrations in the electrolyte solution, where the ionic conductivity of 1 mol/L, 0.1 mol/L and 0.01 mol/L solution corresponds to 7.6 mS/cm, 2.1 mS/cm and 0.34 mS/cm at 25°C, respectively. With decreasing

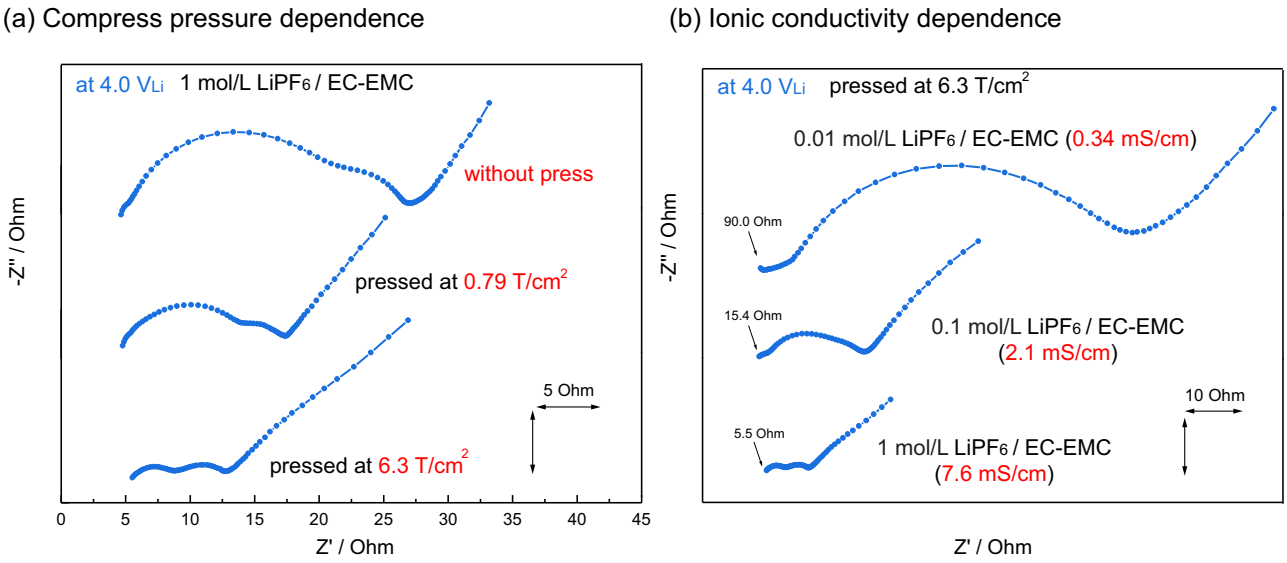

Figure 4. Nyquist plots for a $LiCoO_2$ composite electrode at 4.0 V_{Li} in $LiCoO_2$|$Li_4Ti_5O_{12}$-mesh|Li three electrode cell at 25°C; (a) electrode compress pressure dependence and (b) electrolytes ionic conductivity dependence. Cell was galvanostatically charged at 27.2 mA/g (0.1C) and hold potential for 1 hour at each potential, then relax 1 hour before EIS sequence. Ionic conductivity of electrolytes was measured at 25°C.

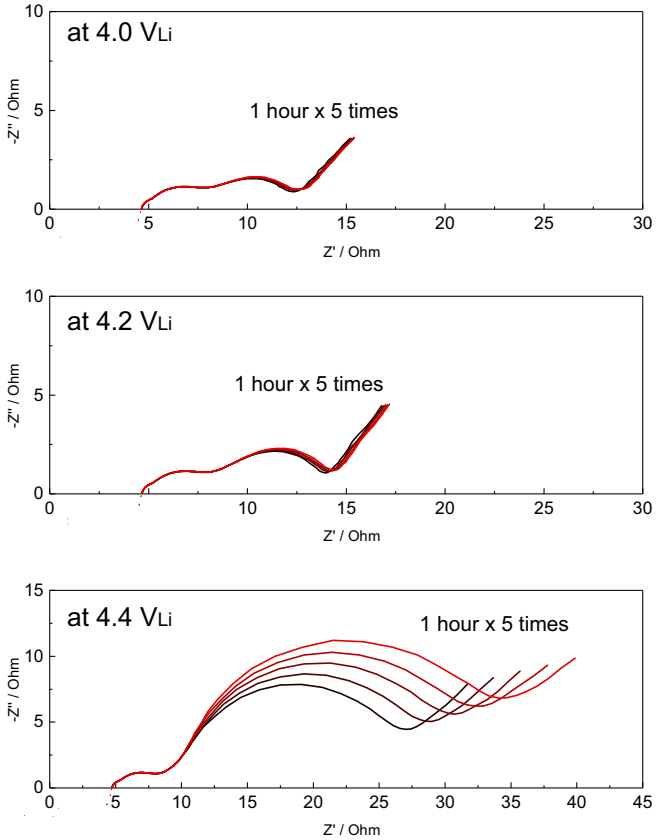

Figure 5. Time dependence of Nyquist plots for a $LiCoO_2$ composite electrode with potential holding at 4.0, 4.2 and 4.4 V_{Li} in $LiCoO_2$|$Li_4Ti_5O_{12}$-mesh|Li three electrode cell at 25°C. EIS measurement was conducted every one hour for five times (black to red line).

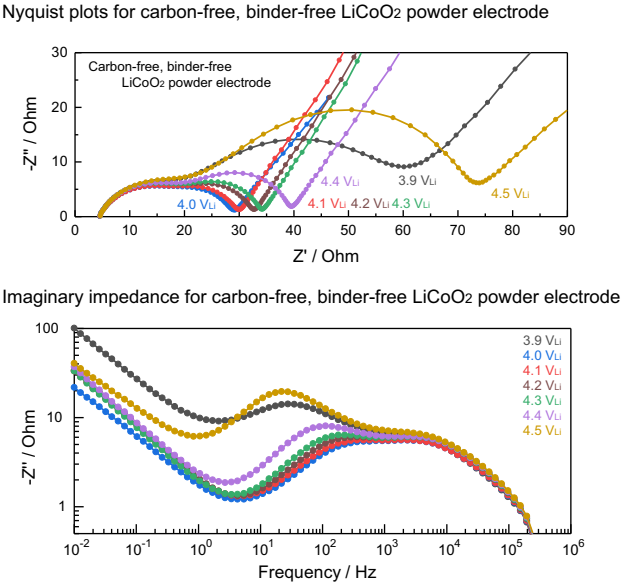

Figure 6. (a) Nyquist plots and (b) frequency dependence of imaginary impedance for carbon-free, binder-free $LiCoO_2$ powder electrode in $LiCoO_2$|$Li_4Ti_5O_{12}$-mesh|Li three electrode cell with 1 mol /L $LiPF_6$ / EC-EMC (3:7 wt/wt) as electrolyte at different potential at 25°C. Cell was galvanostatically charged at 27.2 mA/g (0.1C) and hold potential for 1 hour at each potential, then relax 1 hour before EIS sequence. The $LiCoO_2$ loading is 2.2 mg/cm^2 and $LiCoO_2$ electrode was compressed at 6.3 T/cm^2.

ionic conductivity, both R_{HF} and R_{LF} was increased and almost overlapped at 0.01 mol/L solution. Increase of R_{HF} at lower ionic conductivity can be explained by higher resistance to migrate Li^+ in electrode pore structures. Small bumps in most high-frequency (left) region would come from reference electrode impedance contribution (see experimental section). On the other hand, R_{LF}, which was assigned to charge transfer resistance, should also be increased with decreasing reaction species (Li^+), because charge transfer kinetics can be generally described as $1/R_{ct} \propto c_{Li}{}^{1/2}$ from Butler-Volmer's equation with assuming transference coefficient to be 0.5.[45,46]

Although there are some reports which assign high frequency semicircle to electronic contact resistance of composite electrode (active material particle/particle or particle/current collector, particle/current collector effect is reported to be dominant),[10,13,14,19,47] however, ionic conductivity trends shown in Figure 4b cannot be explained only by electronic contact resistance contribution (contact resistance should not change largely with different electrolytes). Since electrified interface impedance is the combination of electron migration in the composite electrode, Li^+ migration in composite pore structure and Li^+ ion desorption and adsorption on the composite electrode surface, which is in agreement with having R_{HF} of composite electrodes decreasing with increasing both electronic conductance and ionic conductance, and having only one semicircle appeared on EIS at thin film[28] / single particle.[29] Activation energy of each step (high/low frequency) will be discussed in latter part.

EIS measurements with potential holding were conducted at different voltages. Figure 5 shows the time dependence of Nyquist plots for a $LiCoO_2$ composite electrode with potential holding at 4.0, 4.2 and 4.4 V_{Li}. The size of low-frequency (right) semicircle keeps almost constant for 5 hours at 4.0 V_{Li} while it was increased slightly at 4.2 V_{Li}, and significantly at 4.4 V_{Li}. This trend for low-frequency semicircle of Li_xCoO_2 composite electrodes is consistent with comparable results reported for the one semicircle of thin-film[28,44] and single-particle electrodes[29] with potential holding or cycling at similar potentials. We propose that potential holding would increase EEI layer thickness by decomposing more electrolyte (especially above 4.4 V_{Li} on the layered oxide materials such as $LiNi_{0.33}Mn_{0.33}Co_{0.33}O_2$)[7] with time during holding and increase the R_{LF}. Increase of R_{LF} at higher potential implies restricted electrode kinetics due to further electrolyte decomposition occurred on the $LiCoO_2$ surface and forming EEI layer.[3] The increased reactivity of $LiCoO_2$ surface with higher degree of delithiation induces accumulation of decomposition products on the EEI layer and it would suppress charge transfer kinetics (further discussion in later section).[4] Therefore, this increasing trend upon exposure for high potential further supports that low-frequency semicircle in composite electrode can be affected by both charge transfer and EEI layer resistance. In contrast, high-frequency (left) semicircle does not change during potential holding even at 4.4 V_{Li}, suggesting R_{HF} cannot be assigned to EEI layer (so-called surface film) resistance, but to the electrified interface resistance, because it should be reasonably assumed that electrified interface impedance does not change with holding potential.

EIS measurements on carbon-free, binder-free $LiCoO_2$ electrode were also carried out to see the effect of conductive carbon on the behavior (Figure 6). As well as EIS response on composite electrodes (Figure 2), two semicircles can be observed on Nyquist plots for carbon-free, binder-free electrode and each response shows almost the same imaginary impedance peak top frequency (high frequency $\sim 10^4$ Hz, low frequency $\sim 10^1$–10^2 Hz) as composite electrode results. High-frequency semicircles do not change with varying potential while low-frequency semicircles show the same trend as the one with composite electrodes (showing minimum resistance at 4.0 V_{Li}). Consistent with the results from potential holding experiment as discussed above (Figure 5), this observation indicates high-frequency semicircle does not necessarily originate from high-surface area conductive carbon or binder polymer in composite electrode structure. However, both electronic (electron migration via particle) and ionic (Li^+ migration in pore) resistance in composite electrode structure (electrified

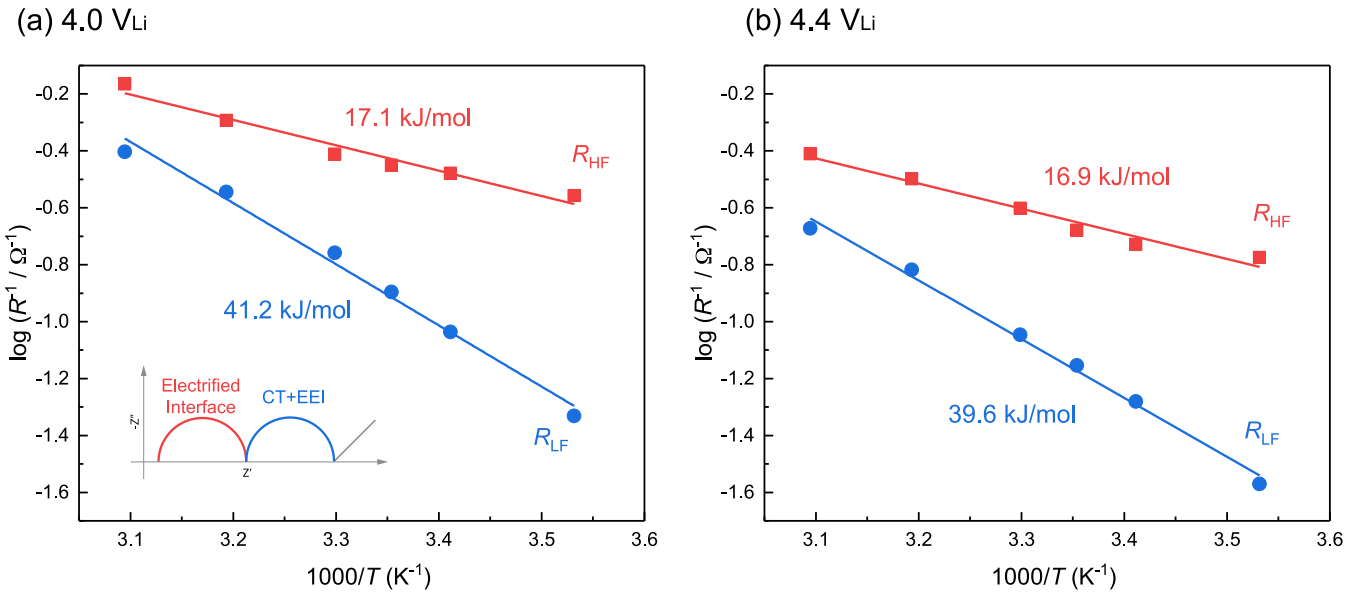

Figure 7. Arrhenius plots of interfacial resistances for a $LiCoO_2$ composite electrode (compressed at 6.3 T/cm^2) at (a) 4.0 and (b) 4.4 V_{Li} in $LiCoO_2$|$Li_4Ti_5O_{12}$-mesh|Li three electrode cell. Original temperature dependent Nyquist plots are shown in Figure S3. Cell was galvanostatically charged at 27.2 mA/g (0.1C) and hold potential for 1 hour at 25°C, then EIS was carried out at open circuit potential at each temperature. Activation energy of electrolyte ionic conduction (ion migration in bulk) are measured as 12.2 kJ/mol (Figure S4). Arrhenius plots with less compressed electrode (0.79 T/cm^2) are available in Figure S5.

interface impedance) affect R_{HF}, because thin film and single particle electrodes, which also do not have conductive carbon and binder polymer, show only one semicircle.[28,29,43,44]

Due to much higher surface roughness of carbon-free, binder-free electrodes (the electrode was prepared by just drop casting of $LiCoO_2$/NMP dispersion, see experimental section), the observed two semicircles cannot be separated so well especially around 4.0–4.3 V_{Li}. In addition, larger impedance compared with the one from composite electrodes might come from lower electric conductivity in the carbon-free, binder-free electrode structure due to lack of conductive carbon, however, it would be challenging to quantitatively compare resistance since the preparation method as well as the surface morphology/smoothness are far different between composite and carbon-free, binder-free electrodes. Therefore, here we simply used composite electrode for following discussion.

The effect of EEI formation to charge transfer kinetics.—To further connect the effect of EEI layer formation to energetics and kinetics for electrode reaction, activation energy was calculated. Figure 7 shows Arrhenius plots of both R_{LF} and R_{HF} at 4.0 and 4.4 V_{Li} (Original temperature dependent Nyquist plots are available in Figure S3). The activation energies (E_a) were evaluated from the slopes of the Arrhenius plots with the Arrhenius equation, $R_{HF/LF}^{-1} = A\exp(-E_a/RT)$, where A denotes frequency factor, R denotes ideal gas constant and T denotes absolute temperature. As shown in Figure 7a, activation energy for R_{LF} at 4.0 V_{Li} was calculated to be 41.2 kJ/mol. This value is comparable with the activation energy of 30–60 kJ/mol for charge transfer reactions, where the desolvation/solvation of Li^+ ion is the rate-determining step.[48] Although the desolvation/solvation energy (i.e. interaction energy) of lithium ions can vary depending on solvent and anion,[49–51] the value in this work is in good agreement with previous work[39] (e.g. 48±6 kJ/mol at $LiCoO_2$ in 1 mol/L $LiCF_3SO_3$ in propylene carbonate), where higher value can be attributed to higher Lewis basicity of $LiCF_3SO_3$ than $LiPF_6$.[51] Activation energy of R_{LF} at 4.4 V_{Li} was also calculated as 39.6 kJ/mol, which can be regarded as the same as the one at 4.0 V_{Li} (41.2 kJ/mol) within typical experimental error for activation energy measurement (± 2–6 kJ/mol).[39,52] Generally speaking, the activation energy of Li^+ ion conduction in inorganic solid state electrolytes is around 40–50 kJ/mol,[53,54] which also shows a good agreement with the value for R_{LF} but not for R_{HF} in this study.

The activation energy of R_{HF}, which was assigned to the impedance for the electrified interface, was calculated to be 17.1 kJ/mol and 16.9 kJ/mol, at 4.0 and 4.4 V_{Li}, respectively. These values are consistent with those reported for R_{HF} by Xu et al.,[55] which are close to the activation energy for ionic conduction in bulk electrolyte solutions such as LP57 (1 mol/L $LiPF_6$ in EC-EMC) in Figure S4 (12.2 kJ/mol). This value is in good agreement with that from Ogihara et al., having the activation energy of ion migration in composite pore structure being 16 kJ/mol.[56] On the other hand, the activation energy of electronic conduction within the composite structure is much lower (nearly temperature independent) than that for ion conduction,[56,57] the high-frequency impedance was attributed to Li^+ ion adsorption onto and desorption from pore surfaces and Li^+ ion migration in the composite electrodes. This hypothesis is further supported by temperature-dependent measurements with less compressed electrode (0.79 T/cm^2, shown in Figure S5), which had a lower activation energy of R_{HF} being 9.8 kJ/mol than that for well-compressed (6.3 T/cm^2) electrodes, reflecting a higher contribution of electronic migration. Therefore, well-compressed electrodes had electrified interface impedance that was mainly governed by Li^+ ion adsorption onto and desorption from pore surfaces and Li^+ ion migration in the composite electrodes.

Activation energy of R_{HF} and R_{LF} was examined with different potential holding time at 4.4 V_{Li} (Figure 8a), where R_{LF} was shown to increase considerably with holding time while R_{HF} remained largely constant for 80 hours. In addition, imaginary impedance plotted against frequency are shown in Figure 8b, where peak frequency in the imaginary impedance describes the time scale of specific processes. Peak top frequency for higher frequency region is almost constant at $f_{max} = \sim 2000$ Hz (time constant: $\tau = 1/(2\pi f_{max}) = \sim 8.0 \times 10^{-5}$ s) for 80 hours, suggesting time scale of electrified interface impedance keeps constant with holding potential over time. However, peak frequency for low-frequency semicircle was shifted to lower frequency from $f_{max} = \sim 5$ Hz ($\tau = \sim 3.2 \times 10^{-2}$ s) at after 1 hour holding, and to $f_{max} = \sim 0.6$ Hz ($\tau = \sim 2.7 \times 10^{-1}$ s) at after 80 hours. This one order of magnitude increase of time constant clearly suggests that the process became slower with holding, which can be attributed to

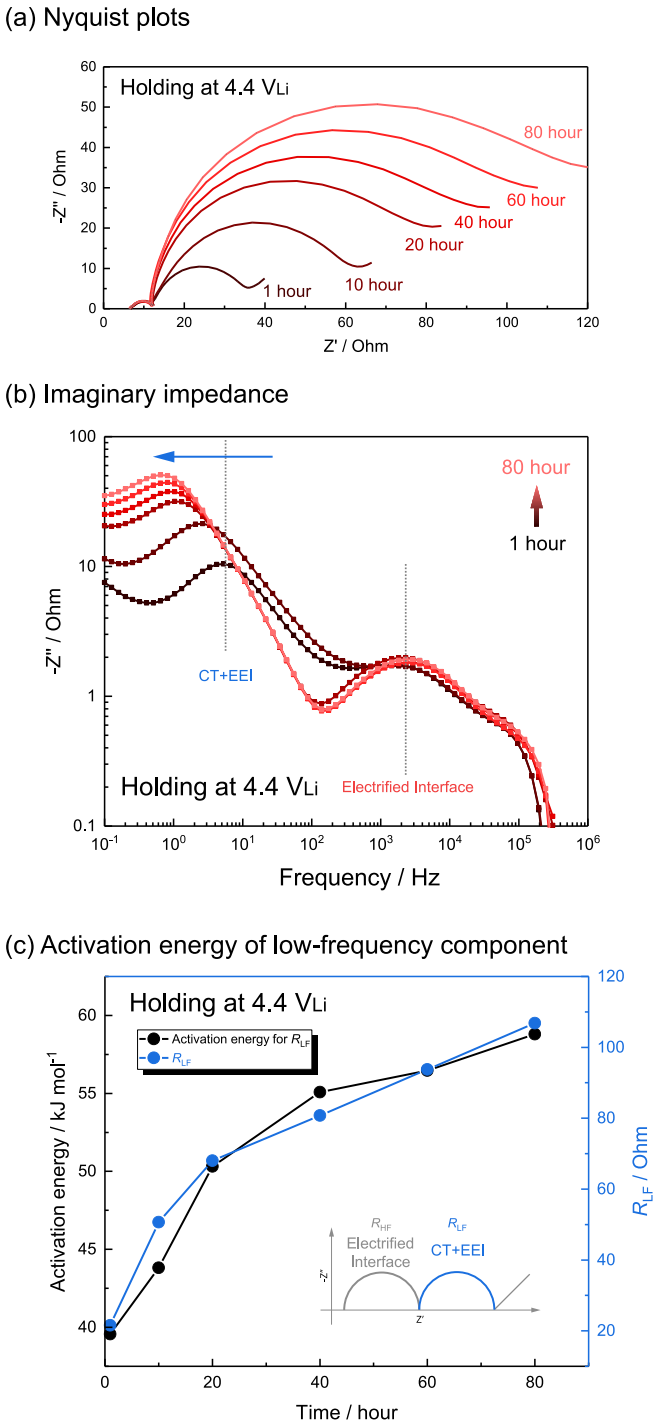

Figure 8. Time dependence of EIS measurement on $LiCoO_2$ composite electrode with holding potential at 4.4 V_{Li} in $LiCoO_2$|$Li_4Ti_5O_{12}$-mesh|Li three electrode cell at 25°C; (a) Nyquist plots, (b) frequency dependence of imaginary impedance and (c) activation energy of low-frequency component.

increased resistance associated with growing EEI layer. Moreover, calculated activation energy of R_{LF} with holding time at 4.4 V_{Li} increased with holding time for 80 hours by a factor of 1.5, from 40 kJ/mol to 60 kJ/mol, not reaching steady-state, as shown in Figure 8c (some Nyquist plots which do not show Warburg tail due to very high R_{LF} were simply fitted by only RQ-element). This observation implies that EEI layer formed at 4.4 V_{Li} might not be fully passivated after 80 hours, however growing rate is slowed down after 20 hours.

In order to verify the EEI layer growth on the electrode surface during potential holding at 4.4 V_{Li}, XPS analysis of C1s, O1s, F1s and P2p was conducted for Li_xCoO_2 composite electrodes before and after holding potential at 4.4 V_{Li} for 1 hour and 80 hours (Figure 9). Figure 9a shows the C1s spectra, which were fitted to component adventitious C-H/C-C (E_b = 285 eV), C-O (and/or PVDF) (E_b~286.3 eV), C=O/O-C-O (E_b~287.6 eV), O=C-O (E_b~288.8 eV) and CO_3 (and/or PVDF) (E_b~290.3 eV). As shown in Figure 9b, the low binding energy component of O1s, which corresponding to the oxygen lattice (~529 eV) of $LiCoO_2$,[58] became smaller with holding potential (bottom to top), indicative of surface film growth on the $LiCoO_2$ surface with hold time[3]. As the penetration depth of laboratory XPS is around 5 nm,[59] the presence of oxygen lattice at 529 eV indicates that formed EEI layer is thinner than ~5nm even after potential holding for 80 hours. In addition, C-O bond observed in C1s (~286.3 eV) in Figure 9a and O1s (~533.4 eV) in Figure 9b was found to increase with potential holding. This C-O component indicates the presence of oligomers (such as polyethylene oxide) due to electrolyte oxidation/decomposition at high potential.[60,61] C-O band was previously observed in XPS on carbon-free, binder-free electrodes,[3] however, XPS on composite electrode obtained here shows much higher intensity for C-O component, suggesting not only electrolyte but also conductive carbon was oxidized at higher potentials. Moreover, LiF (~685.1 eV in F1s) and lithiated fluorophosphates ($Li_xPF_yO_z$, ~686.6 eV in F1s and 136 eV in P2p), which are known as major components of EEI layer on the $LiCoO_2$ surface,[3,62] were found after 1 hour potential holding at 4.4 V_{Li}, as shown in the F 1s spectra in Figure 9c and P2p in Figure 9d. Furthermore, after 80 hours of potential holding, lithiated fluorophosphates ($Li_xPF_yO_z$) in P2p, drastically increased from 1 hour to 80 hours. These observations support that the EEI layer (LiF, $Li_xPF_yO_z$, oligomers) grew and became increasingly resistive to lithium ion conduction with holding potential, which is in agreement with activation energy increase in Figure 8. Therefore, the increased reactivity of $LiCoO_2$ surface with higher degree of delithiation (i.e. 4.4 V_{Li}) and holding potential there can accumulate decomposition products on the EEI layer (the increase of oligomer and salt related species such as $Li_xPF_yO_z$) and suppress charge transfer kinetics.[3,4]

Conclusions

We have proposed here the assignment of electrochemical impedance spectra for composite positive electrode in Li-ion battery. The spectra have been modeled following rigorous criteria via experimental approach (schematically shown in Figure 3). High-frequency semicircle can be assigned to impedance at the electrified interface, where lithium ion adsorption/desorption on the surface of composite pore structure coupled with lithium ion migration in the pore. Low-frequency semicircle should correspond to the combination of charge transfer resistance of lithium de-solvation/solvation and lithium intercalation/deintercalation to/from the active particle surface, and lithium migration through the EEI layer resistance during charge transfer. Composite electrode showed two semicircles, on the other hand, only one semicircle appeared on the EIS for thin film electrode due to the absence of particle/pore structure. More importantly, with increasing EEI layer thickness, the resistance for low-frequency components was increased as well as its activation energy. These observations indicate energetic barrier to proceed charge transfer through EEI layer increased with EEI layer growth, suppressing the kinetics of the entire process. The insights obtained here should enable new strategies for probing the effect of EEI layer on kinetics of electrochemical interfacial reactions.

Acknowledgments

This work was financially supported by BMW Group. This work made use of the MRSEC Shared Experimental Facilities at MIT (XPS and SEM), supported by the National Science Foundation under award

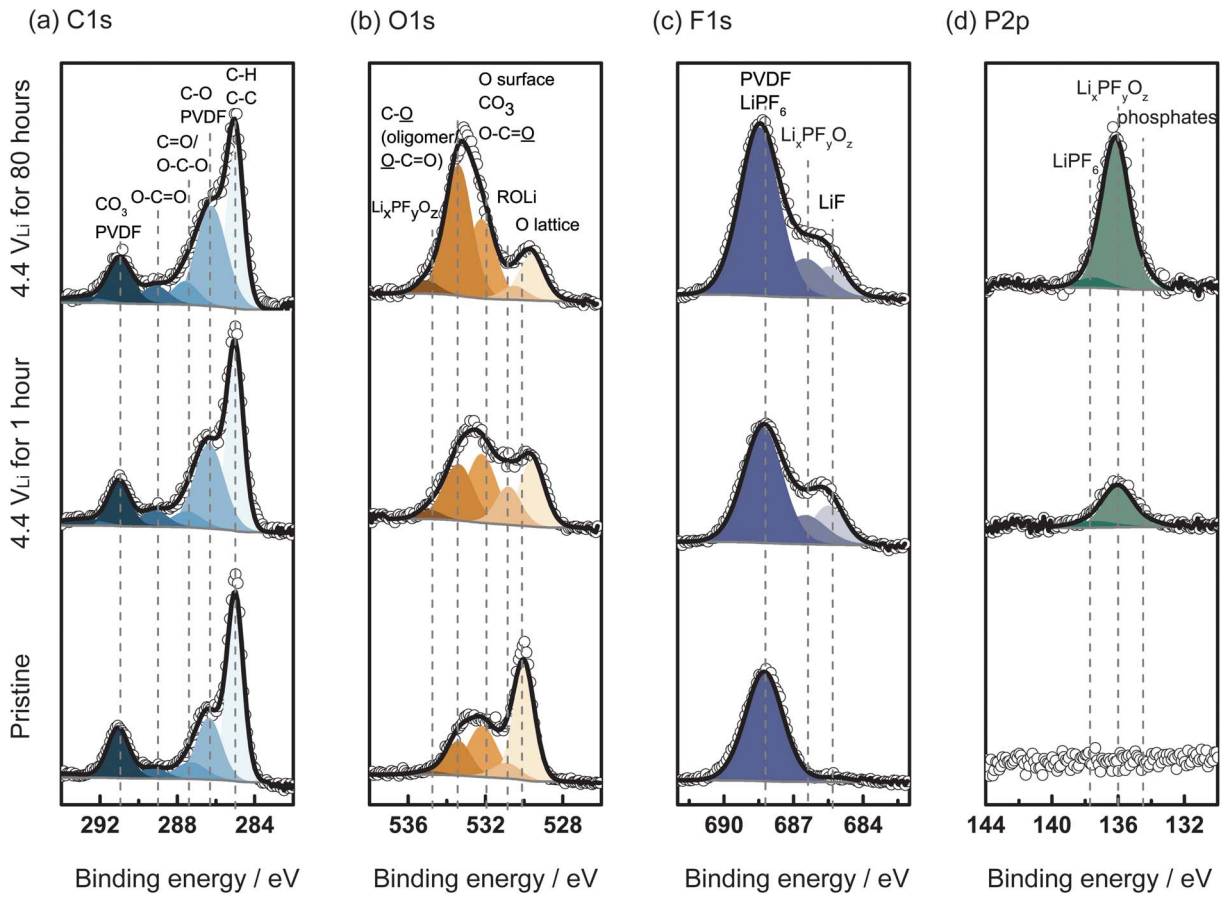

Figure 9. XPS spectra of the (a) C1s, (b) O1s, (c) F1s and (d) P2p photoemission lines collected from composite Li_xCoO_2 electrodes. The electrodes were charged to 4.4 V_{Li} at 27.2 mA/g (0.1C) and hold at 4.4 V_{Li} for 1 hour and 80 hours using 1 mol/L $LiPF_6$ in EC: EMC (3:7 wt:wt) and compared with pristine electrode. All spectra were calibrated with the C1s photoemission peak of adventitious carbon at 285 eV. After subtraction of a Shirley-type background, all the spectra were normalized by fixing the C1s photoemission peak of adventitious carbon (285 eV) to the same value to facilitate comparison between samples. The spectra were assigned with the following contributions.[3] C1s: C-H/C-C (E_b=285 eV), C-O (and/or PVDF) (E_b~286.3 eV), C=O/O-C-O (E_b~287.6 eV), O=C-O (E_b~288.8 eV) and CO_3 (and/or PVDF) (E_b~290.3 eV). O1s: O lattice (E_b~529.3 eV), ROLi (E_b~531 eV), surface O/CO_3/O-C=O (E_b~532 eV), C-O/O-C=O (E_b~533.4 eV) and $Li_xPF_yO_z$ (E_b~534.8 eV). F1s: LiF (E_b~685.1 eV), $Li_xPF_yO_z$ (E_b~686.6 eV) and $LiPF_6$ (and/or PVDF) (E_b~688.3 eV). P2p: phosphates (E_b~134 eV), $Li_xPF_yO_z$ (E_b~136 eV) and $LiPF_6$ (E_b~137.7 eV).

number DMR-1419807. RT thanks Dr. Dino Klotz for his helpful EIS workshop and technical assistance to design the EIS cell.

ORCID

Ryoichi Tatara https://orcid.org/0000-0002-8148-5294
Yang Shao-Horn https://orcid.org/0000-0001-8714-2121

References

1. M. Gauthier, T. J. Carney, A. Grimaud, L. Giordano, N. Pour, H. H. Chang, D. P. Fenning, S. F. Lux, O. Paschos, C. Bauer, F. Maglia, S. Lupart, P. Lamp, and Y. Shao-Horn, *J. Phys. Chem. Lett.*, **6**(22), 4653 (2015).
2. R. Fong, U. V. Sacken, and J. R. Dahn, *J. Electrochem. Soc.*, **137**(7), 2009 (1990).
3. M. Gauthier, P. Karayaylali, L. Giordano, S. Feng, S. F. Lux, F. Maglia, P. Lamp, and Y. Shao-Horn, *J. Electrochem. Soc.*, **165**(7), A1377 (2018).
4. L. Giordano, P. Karayaylali, Y. Yu, Y. Katayama, F. Maglia, S. Lux, and Y. Shao-Horn, *J. Phys. Chem. Lett.*, **8**(16), 3881 (2017).
5. R. Jung, M. Metzger, F. Maglia, C. Stinner, and H. A. Gasteiger, *J. Electrochem. Soc.*, **164**(7), A1361 (2017).
6. R. Jung, R. Morasch, P. Karayaylali, K. Phillips, F. Maglia, C. Stinner, Y. Shao-Horn, and H. A. Gasteiger, *J. Electrochem. Soc.*, **165**(2), A132 (2018).
7. Y. Yu, P. Karayaylali, Y. Katayama, L. Giordano, M. Gauthier, F. Maglia, R. Jung, I. Lund, and Y. Shao-Horn, *J. Phys. Chem. C*, in press, (2018).
8. M. G. S. R. Thomas, P. G. Bruce, and J. B. Goodenough, *J. Electrochem. Soc.*, **132**(7), 1521 (1985).
9. D. Aurbach, M. D. Levi, Levi Elena, H. Teller, B. Markovsky, G. Salitra, U. Heider, and L. Herder, *J. Electrochem. Soc.*, **145**(9), 3024 (1998).
10. H. Nara, K. Morita, D. Mukoyama, T. Yokoshima, T. Momma, and T. Osaka, *Electrochim. Acta*, **241**, 323 (2017).
11. M. D. Levi and D. Aurbach, *J. Phys. Chem. B*, **101**(23), 4630 (1997).
12. H. Zheng, K. Jiang, T. Abe, and Z. Ogumi, *Carbon*, **44**(2), 203 (2006).
13. Y.-M. Choi, S.-I. Pyun, J.-S. Bae, and S.-I. Moon, *J. Power Sources*, **56**(1), 25 (1995).
14. A.-K. Hjelm and G. Lindbergh, *Electrochim. Acta*, **47**(11), 1747 (2002).
15. Y. Yamada, Y. Iriyama, T. Abe, and Z. Ogumi, *J. Electrochem. Soc.*, **157**(1), A26 (2010).
16. T. Abe, F. Sagane, M. Ohtsuka, Y. Iriyama, and Z. Ogumi, *J. Electrochem. Soc.*, **152**(11), A2151 (2005).
17. M. D. Levi and D. Aurbach, *J. Phys. Chem. B*, **101**(23), 4641 (1997).
18. D. Aurbach, M. D. Levi, E. Levi, and A. Schechter, *J. Phys. Chem. B*, **101**(12), 2195 (1997).
19. M. Gaberscek, J. Moskon, B. Erjavec, R. Dominko, and J. Jamnik, *Electrochem. Solid-State Lett.*, **11**(10), A170 (2008).
20. S. J. An, J. Li, Y. Sheng, C. Daniel, and D. L. Wood, *J. Electrochem. Soc.*, **163**(14), A2866 (2016).
21. H. Zheng, H. Zhang, Y. Fu, T. Abe, and Z. Ogumi, *J. Phys. Chem. B*, **109**(28), 13676 (2005).
22. L. Xia, K. Qiu, Y. Gao, X. He, and F. Zhou, *J. Mater. Sci.*, **50**(7), 2914 (2015).
23. S. S. Zhang, K. Xu, and T. R. Jow, *Electrochim. Acta*, **51**(8–9), 1636 (2006).
24. S. J. An, J. Li, Z. Du, C. Daniel, and D. L. Wood, *J. Power Sources*, **342**, 846 (2017).
25. M. Ender, J. Illig, and E. Ivers-Tiffée, *J. Electrochem. Soc.*, **164**(2), A71 (2016).
26. J. Costard, M. Ender, M. Weiss, and E. Ivers-Tiffée, *J. Electrochem. Soc.*, **164**(2), A80 (2016).
27. S. Solchenbach, D. Pritzl, E. J. Y. Kong, J. Landesfeind, and H. A. Gasteiger, *J. Electrochem. Soc.*, **163**(10), A2265 (2016).
28. D. Takamatsu, Y. Koyama, Y. Orikasa, S. Mori, T. Nakatsutsumi, T. Hirano, H. Tanida, H. Arai, Y. Uchimoto, and Z. Ogumi, *Angew. Chem. Int. Ed.*, **51**(46), 11597 (2012).

29. K. Dokko, M. Mohamedi, Y. Fujita, T. Itoh, M. Nishizawa, M. Umeda, and I. Uchida, *J. Electrochem. Soc.*, **148**(5), A422 (2001).
30. T. Osaka, D. Mukoyama, and H. Nara, *J. Electrochem. Soc.*, **162**(14), A2529 (2015).
31. Y. Hoshi, Y. Narita, K. Honda, T. Ohtaki, I. Shitanda, and M. Itagaki, *J. Power Sources*, **288**, 168 (2015).
32. R. Younesi, A. S. Christiansen, R. Scipioni, D. T. Ngo, S. B. Simonsen, K. Edstrom, J. Hjelm, and P. Norby, *J. Electrochem. Soc.*, **162**(7), A1289 (2015).
33. E. Endo, T. Yasuda, A. Kita, K. Yamaura, and K. Sekai, *J. Electrochem. Soc.*, **147**(4), 1291 (2000).
34. Z. Chen and J. R. Dahn, *Electrochim. Acta*, **49**(7), 1079 (2004).
35. Y. Ozawa, R. Yazami, and B. Fultz, *J. Power Sources*, **119–121**, 918 (2003).
36. S. S. Zhang, K. Xu, and T. R. Jow, *Electrochim. Acta*, **49**(7), 1057 (2004).
37. I. Landa-Medrano, I. Ruiz de Larramendi, N. Ortiz-Vitoriano, R. Pinedo, J. Ignacio Ruiz de Larramendi, and T. Rojo, *J. Power Sources*, **249**, 110 (2014).
38. J. Illig, M. Ender, T. Chrobak, J. P. Schmidt, D. Klotz, and E. Ivers-Tiffée, *J. Electrochem. Soc.*, **159**(7), A952 (2012).
39. I. Yamada, Y. Iriyama, T. Abe, and Z. Ogumi, *J. Power Sources*, **172**(2), 933 (2007).
40. S. Yamada, M. Fujiwara, and M. Kanda, *J. Power Sources*, **54**(2), 209 (1995).
41. H. Xia, L. Lu, and G. Ceder, *J. Power Sources*, **159**(2), 1422 (2006).
42. I. Yamada, T. Abe, Y. Iriyama, and Z. Ogumi, *Electrochem. Commun.*, **5**(6), 502 (2003).
43. H. Sato, D. Takahashi, T. Nishina, and I. Uchida, *J. Power Sources*, **68**(2), 540 (1997).
44. D. Takamatsu, Y. Orikasa, S. Mori, T. Nakatsutsumi, K. Yamamoto, Y. Koyama, T. Minato, T. Hirano, H. Tanida, H. Arai, Y. Uchimoto, and Z. Ogumi, *J. Phys. Chem. C*, **119**(18), 9791 (2015).
45. D. Takamatsu, S. Mori, Y. Orikasa, T. Nakatsutsumi, Y. Koyama, H. Tanida, H. Arai, Y. Uchimoto, and Z. Ogumi, *J. Electrochem. Soc.*, **160**(5), A3054 (2013).
46. S. Kobayashi and Y. Uchimoto, *J. Phys. Chem. B*, **109**(27), 13322 (2005).
47. S.-S. Kim, Y. Kadoma, H. Ikuta, Y. Uchimoto, and M. Wakihara, *Electrochem. Solid-State Lett.*, **4**(8), A109 (2001).
48. Y. Yamada, Y. Iriyama, T. Abe, and Z. Ogumi, *Langmuir*, **25**(21), 12766 (2009).
49. D. G. Kwabi, V. S. Bryantsev, T. P. Batcho, D. M. Itkis, C. V. Thompson, and Y. Shao-Horn, *Angew. Chem. Int. Ed.*, **55**(9), 3129 (2016).
50. K. Ueno, K. Yoshida, M. Tsuchiya, N. Tachikawa, K. Dokko, and M. Watanabe, *J. Phys. Chem. B*, **116**(36), 11323 (2012).
51. M. Schmeisser, P. Illner, R. Puchta, A. Zahl, and R. van Eldik, *Chem. Eur. J.*, **18**(35), 10969 (2012).
52. T. Doi, K. Miyatake, Y. Iriyama, T. Abe, Z. Ogumi, and T. Nishizawa, *Carbon*, **42**(15), 3183 (2004).
53. J. C. Bachman, S. Muy, A. Grimaud, H. H. Chang, N. Pour, S. F. Lux, O. Paschos, F. Maglia, S. Lupart, P. Lamp, L. Giordano, and Y. Shao-Horn, *Chem. Rev.*, **116**(1), 140 (2016).
54. S. Muy, J. C. Bachman, H.-H. Chang, L. Giordano, F. Maglia, S. Lupart, P. Lamp, W. G. Zeier, and Y. Shao-Horn, *Chem. Mater.*, **30**(16), 5573 (2018).
55. K. Xu, Y. Lam, S. S. Zhang, T. R. Jow, and T. B. Curtis, *J. Phys. Chem. C*, **111**(20), 7411 (2007).
56. N. Ogihara, S. Kawauchi, C. Okuda, Y. Itou, Y. Takeuchi, and Y. Ukyo, *J. Electrochem. Soc.*, **159**(7), A1034 (2012).
57. J. P. Schmidt, T. Chrobak, M. Ender, J. Illig, D. Klotz, and E. Ivers-Tiffée, *J. Power Sources*, **196**(12), 5342 (2011).
58. S. Verdier, L. El Ouatani, R. Dedryveàre, F. Bonhomme, P. Biensan, and D. Gonbeau, *J. Electrochem. Soc.*, **154**(12), A1088 (2007).
59. D. Briggs and J. T. Grant, *Surface analysis by Auger and X-ray photoelectron spectroscopy*, IMPublications (2003).
60. R. Dedryvère, H. Martinez, S. Leroy, D. Lemordant, F. Bonhomme, P. Biensan, and D. Gonbeau, *J. Power Sources*, **174**(2), 462 (2007).
61. R. A. Quinlan, Y.-C. Lu, D. Kwabi, Y. Shao-Horn, and A. N. Mansour, *J. Electrochem. Soc.*, **163**(2), A300 (2015).
62. Y.-C. Lu, A. N. Mansour, N. Yabuuchi, and Y. Shao-Horn, *Chem. Mater.*, **21**(19), 4408 (2009).